Ridge migration, asthenospheric flow and the origin of magmatic segmentation in the global mid-ocean ridge system

Richard F. Katz, Marc Spiegelman, and Suzanne M. Carbotte

Lamont-Doherty Earth Observatory, Columbia University, Palisades, New York, USA

[1] Global observations of mid-ocean ridge (MOR) bathymetry demonstrate an asymmetry in axial depth across ridge offsets that is correlated with the direction of ridge migration. Motivated by these observations, we have developed two-dimensional numerical models of asthenospheric flow and melting beneath a migrating MOR. The modification of the flow pattern produced by ridge migration leads to an asymmetry in melt production rates on either side of the ridge. By coupling a simple parametric model of three dimensional melt focusing to our simulations, we generate predictions of axial depth differences across offsets in the MOR. These predictions are quantitatively consistent with the observed asymmetry. *INDEX TERMS:* 3040 Marine Geology and Geophysics: Plate tectonics (8150, 8155, 8157, 8158); 3210 Mathematical Geophysics: Modeling; 8120 Tectonophysics: Dynamics of lithosphere and mantle—general; 8162 Tectonophysics: Rheology—mantle; 8434 Volcanology: Magma migration. **Citation:** Katz, R. F., M. Spiegelman, and S. M. Carbotte (2004), Ridge migration, asthenospheric flow and the origin of magmatic segmentation in the global mid-ocean ridge system, *Geophys. Res. Lett.*, *31*, L15605, doi:10.1029/2004GL020388.

1. Introduction

[2] Global observations of the bathymetry of intermediate and fast spreading mid-ocean ridges (MOR) by *Carbotte et al.* [2004] demonstrate that differences in axial depth across ridge offsets are correlated with the direction of ridge migration in the fixed hot-spot reference frame. They show that the shallower segment across an offset is usually the segment *leading* with respect to the direction of ridge migration (Figure 1a). The systematic connection with plate kinematics, global scope and ubiquity of this observed asymmetry suggests that it might yield to a simple explanation related to plate induced dynamics. Changes in ridge morphology along a MOR are commonly attributed to differences in the volume of melt delivered from the mantle although the origin of these variations in magma supply are poorly understood [*Macdonald et al.*, 1988; *Lin and Phipps-Morgan*, 1992]. *Carbotte et al.* [2004] suggest a conceptual model of melt generation and 3D focusing to account for their observations. They propose that ridge migration leads to asymmetry in mantle upwelling and melt generation with melt production augmented beneath the leading plate and diminished beneath the trailing plate. We quantify this suggestion by calculating the influence of ridge migration on mantle melt production using 2D numerical simulations of asthenospheric flow and adiabatic melting.

[3] Previous authors have considered the possible effect of ridge migration on MOR processes. A kinematic model of asthenospheric flow beneath a migrating ridge was used by *Davis and Karsten* [1986] to explain the asymmetric distribution of seamounts about the Juan de Fuca ridge and by *Schouten et al.* [1987] to study the migration of non-transform offsets at spreading centers. Modeling studies [*Conder et al.*, 2002; *Toomey et al.*, 2002] of the MELT region of the EPR [*Forsyth et al.*, 1998b] found the dynamic effect of ridge migration could produce an asymmetry in melt production, but not of the magnitude inferred from across-ridge differences in P, S and Rayleigh wave velocities [*Forsyth et al.*, 1998a; *Toomey et al.*, 1998] and in electrical conductivity [*Evans et al.*, 1999]. These studies attribute the observed asymmetry in mantle structure to enhanced horizontal flow from a large-scale pressure gradient in the asthenosphere from the distant South Pacific Superswell and additionally, by *Toomey et al.* [2002], to an anomalous asthenospheric temperature inflow. Such considerations may be necessary to explain the large asymmetry seen in the MELT region (assuming the asymmetry is due to melt production) but they represent a geographically special case.

[4] We show that the more general situation of asymmetry generated by ridge migration alone is sufficient to explain the global observations of variation in ridge bathymetry. We describe how shear induced by the relative motion of the lithosphere over the mantle produces an asymmetric perturbation of melt production rates. Furthermore, our model quantitatively predicts the observed relationship between axial depth differences across an offset in the ridge and the length of the offset (Figure 2). Our model is different from those used in previous studies in that it employs a non-Newtonian combined diffusion and dislocation creep viscosity. This viscosity enhances the melting rate asymmetry by a factor of 3 to 4 over diffusion creep alone.

2. Model Description and Solution

[5] Figure 1a shows a conceptual model of three-dimensional melt focusing from the upwelling zone of two adjacent ridge segments separated by a discontinuity. Delivery of melt to the ridge axis is assumed to occur by buoyant flow along a sloping, thermally imposed impermeable barrier [*Magde and Sparks*, 1997]. If the symmetry of the lithospheric thermal structure is not affected by ridge migration, one would expect that the focusing process would be equally efficient to both ridge segments across a ridge discontinuity. Thus, an asymmetry in magma supply inferred from ridge morphology requires a difference in melt production in the regions from which the melt is drawn.
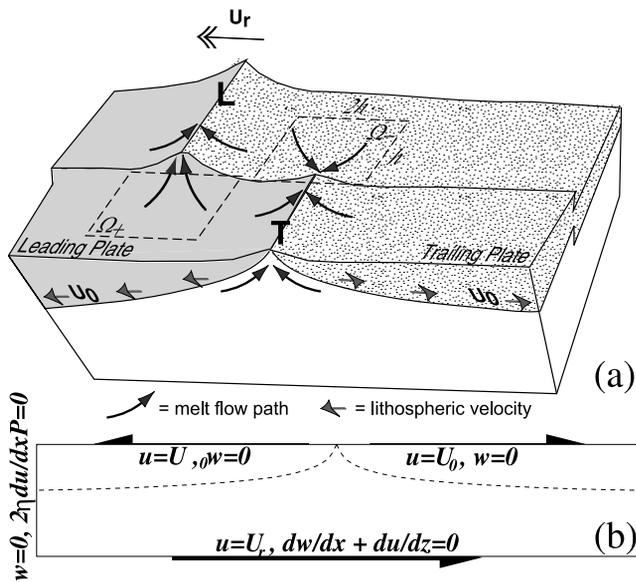
Figure 1. (a) Schematic diagram illustrating a discontinuity in the spreading ridge modified from *Carbotte et al.* [2004]. The ridge-normal rate of ridge migration is given by the vector U_r. The leading segment is labeled **L** and the trailing one **T**. Black arrows show assumed paths of melt focusing beneath the lithosphere. Grey arrows show lithospheric motion. Focusing regions Ω_+ and Ω_- used in equation (3) are dashed rectangles with sides of length h and $2h$. (b) Schematic diagram illustrating the model domain and boundary conditions. Half spreading rate is U_0.

[6] While computing melt focusing near a ridge offset requires a 3D model, the asymmetric production of melt can be investigated in 2D. Here we solve the equations,

$$\nabla P = \nabla \cdot \left[\eta \left(\nabla \mathbf{V} + \nabla \mathbf{V}^T \right) \right]; \quad \text{s.t. } \nabla \cdot \mathbf{V} = 0, \quad (1)$$

$$\mathbf{V} \cdot \nabla \theta = \kappa \nabla^2 \theta, \quad (2)$$

for the thermal and flow structure in the reference frame of the migrating ridge. Here P is the dynamic pressure, θ is the potential temperature and $\mathbf{V}$ is the two dimensional velocity. The viscosity is given by $\eta = (1/\eta_{disl} + 1/\eta_{difn})^{-1}$ where η_{disl} and η_{difn} correspond to P and T-dependent diffusion creep and P, T and strain rate-dependent dislocation creep [*Karato and Wu*, 1993; *Hirth and Kohlstedt*, 2003]. We use values of 14 and 5 cm^3/mole for V^*_{disl} and V^*_{difn}.

[7] In our simulations the asthenospheric depth is equal to the domain depth. The underlying mantle has zero horizontal velocity in the fixed hot-spot frame. A large drop in horizontal mantle velocity with increasing depth is expected across the transition zone for mantle convection with a low viscosity asthenosphere [*Richards et al.*, 2003]. The horizontal velocity on the bottom boundary, however, is set to the ridge migration rate, U_r, because we solve for the flow field in a reference frame fixed to the migrating ridge. Other boundary conditions are illustrated in Figure 1b. The full system of equations and boundary conditions is solved iteratively with a Newton-Krylov-Schwarz method available through the Portable Extensible Toolkit for Scientific Computation (PETSc) [*Balay et al.*, 1997, 2002] (see also http://www.mcs.anl.gov/petsc).

[8] Observations by *Small and Danyushevsky* [2003] show that the mean ratio of the ridge-perpendicular migration rate to the half spreading rate at all ridges studied in Figure 2 is 0.95 with a standard deviation of 0.33. Thus we set the ridge migration rate U_r equal to the half spreading rate U_0 for all model runs. The flow perturbation caused by ridge migration is extracted by subtracting the flow field calculated for a non-migrating ridge from that of an identical calculation with non-zero U_r. Example output is shown in Figure 3.

3. Melting and Melt Focusing

[9] Assuming mantle upwelling to be an isenthalpic process we compute the melting rate *anomaly* due to ridge migration (kg m^{-3} sec^{-1} per kilometer in the along axis direction) as $\Gamma'(x, z) = \rho_m W' dF/dz|_s$ where ρ_m is the density of solid mantle, W' is the vertical velocity perturbation, and $dF/dz|_s$ is the adiabatic productivity. The productivity is computed using a parameterization of mantle melting by *Katz et al.* [2003], assuming a mantle potential temperature of 1300°C. Because this productivity is nearly constant at 0.2 %/km over the melting region and for each of the runs,
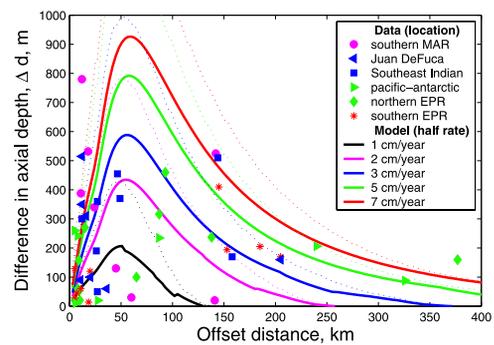

Figure 2. Model results and observations of morphological asymmetry versus offset length of discontinuities in the MOR. **Symbols:** difference in axial depth of two adjacent ridge segments across ridge-axis discontinuities (Δd) restricted to those cases where the leading ridge segment is shallower than the trailing segment. Data for fast and intermediate spreading ridges from *Carbotte et al.* [2004]. Also shown are previously unpublished data from the slow spreading southern MAR 23°–36°S measured as the difference in axis elevation at mid-points of adjacent segments. Along the 11000 km of MOR examined in the combined data set, the leading ridge segments are shallower at 76% of all discontinuities with offsets greater than 5 km. Symbols for each ridge are colored to correspond to the closest model half rate. Mean half rates in cm/year are 1.9 (southern MAR), 2.8 (Juan de Fuca), 3.7 (Southeast Indian), 4.3 (Pacific Antarctic), 4.6 (northern EPR) and 7.0 (southern EPR) [*DeMets et al.*, 1994]. **Curves:** Δd from equation (3) for a range of spreading rates. Solid curves represent a conservative estimate of 670 km for the asthenospheric depth and recover a reasonable melt focusing region, Ω (shown in Figure 1a), determined by approximate "by eye" fitting of the curves to the data. This procedure gives a characteristic dimension h of 24 km, although this solution is non-unique (see text). Dotted curves were computed for an asthenospheric depth limit of 300 km and the same focusing region.
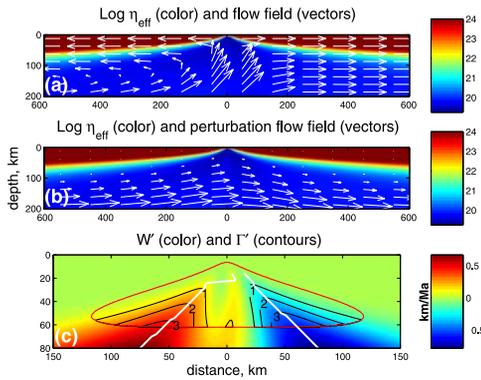
Figure 3. Output from a sample calculation with $U_0 = U_r = 1$ cm/year and domain size of 200 km depth by 1200 km width. **(a)** Colored field is $\log_{10}$ of the viscosity field. Vectors represent the flow pattern beneath the migrating ridge. **(b)** Colored field as in (a). Vectors represent the perturbations of the solid flow field caused by ridge migration. The scaling of the vectors is slightly different in (a) and (b). **(c)** Colored field is W', the vertical component of the velocity perturbation field in km/Ma. The red contour shows the boundary of the melting region and black contours map Γ', the melting rate perturbation, in kg m^{-3} Ma^{-1}. White lines mark the location of the maximal values of W' as a function of depth, as in Figure 4a.

Γ' can be considered a function of W' only. To estimate the axial depth anomaly expected across a discontinuity (e.g., Figure 1a), we integrate Γ' over an area Ω where melt is assumed to be focused to the axis. The predicted difference in crustal thickness, ΔH, is then the difference between the crustal thickness anomalies at leading and trailing segment ends given by:

$$\Delta H = \int \left(\frac{\int_{\Omega^+} \Gamma' dA - \int_{\Omega^-} \Gamma' dA}{2\rho_c U_0} \right) dz \qquad (3)$$

where ρ_c is the density of the crust and U_0 is the half spreading rate. Assuming isostatically compensated topography and crustal density of 2700 kg/m^3, the difference in axial depth, Δd, is equal to approximately $0.26\Delta H$ [*Turcotte and Schubert*, 2002].

4. Results

[10] Figure 3 shows that ridge migration produces asymmetry in the melting rate in 2D calculations. The difference in melt production across the ridge axis increases with spreading rate. For a domain of 670 km depth it ranges from 1% of the total melt production rate for U_0 of 1 cm/yr, to 5% at 3 cm/yr, to 11% at 7 cm/yr. Predicted asymmetry in axial depth computed from these simulations are shown with global ridge data in Figure 2. The curves in this figure are generated using equation (3), adjusted for isostatic compensation. For moderate to fast spreading (greater than 3 cm/year half rate), the model predicts that asymmetry in axial depth has a maximum when the offset length is about 50 km and is still evident when offsets are greater than 200 km. Slower spreading rates result in a peak

asymmetry at slightly smaller distances and zero asymmetry beyond an offset of about 100 km. These model results are consistent with observed differences in ridge elevation as a function of ridge offset length from the moderate to fast spreading ridges examined in *Carbotte et al.* [2004] as well as from the slowly spreading southern Mid Atlantic Ridge (MAR) (Figure 2). The largest contrasts in ridge elevation for the southern MAR occur at transform offsets of less than 50 km and rapidly diminish at longer offsets. Faster spreading ridges show a maximum asymmetry in ridge morphology at longer transform faults of about 50–100 km and smaller amounts of asymmetry at longer offsets.

[11] The solid curves in Figure 2 are computed with a pooling region Ω of size $h = 24$ km, chosen to roughly fit the data (h is defined in Figure 1a). Although there is scatter in the data, our model can account for the general trend and amplitude. The amplitude of the model curves scales inversely with the asthenosphere depth and directly with the area within the pooling region. Both of these parameters are poorly constrained and may vary considerably over the global mid-ocean ridge system. Our estimate of the characteristic distance of melt focusing, h, is thus non-unique. It depends on our assumption of asthenospheric depth of 670 km. A thinner asthenosphere would produce a greater 2D melting asymmetry and thus require a smaller melt focusing region, Ω. The sensitivity of amplitude could be a source of the observed scatter in the data, along with mantle fertility, local spreading rate, deviation of the ratio of half spreading rate to migration rate from unity, etc. However, the shape of the curves and the position of their maxima are independent of these poorly constrained parameters.

5. Discussion

[12] The behavior of the model is readily understood by considering just the component of mantle flow induced by ridge migration (Figure 3b). If there were no lithospheric plates, this additional flow would be simple shear with no vertical velocity component. However, because the lithosphere provides a boundary that curves upward beneath the ridge, the perturbed flow has a vertical component with upwelling on the leading side of the ridge and downwelling on the trailing side. This enhanced vertical flow translates to more melt production on the leading side (Figure 3c). Note that with increasing depth, the location of the maximum (or minimum) of the perturbed melting rate field moves away from the ridge axis along the bold lines shown in Figure 3c. The maximum excess melt production occurs near the intersection of this line with the depth of the solidus, which in this calculation occurs about 50 km off axis.

[13] Figure 4a shows the positions of the extremal lines and the lithospheric thickness for a range of spreading rates from a simplified model that calculates only the perturbed flow due to ridge migration. This figure suggests that for a constant depth solidus, the position of the peak in excess melt production is reasonably insensitive to spreading rate (and should occur roughly at a distance comparable to the depth of the solidus). This result explains the stable position of the peak in Figure 2.

[14] The amplitude of the perturbation in melt production, however, depends on the rate of ridge migration and spreading. Figure 4b shows the value of $|W'|$ as a function
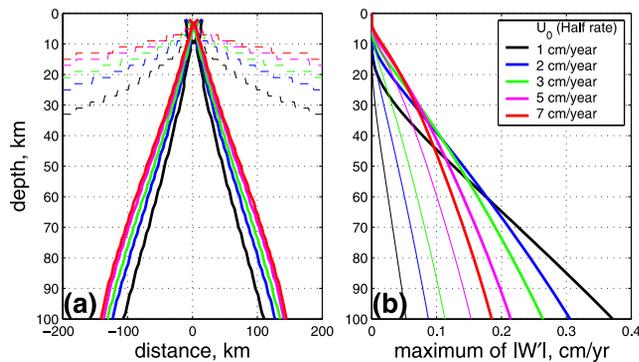
Figure 4. Results from a simplified model for the perturbed flow, showing the effect of spreading rate on the position and magnitude of the peak upwelling perturbation. Model domain is 200 km deep by 800 km wide. **(a)** Dashed curves show the position of the bottom of the lithosphere for calculations at different spreading rates and $U_r = 7$ cm/year (see legend in b). Solid curves show the position, at each depth, of the maximum and minimum in the vertical component of the velocity perturbation field (e.g., see Figure 3). Note that the W' field contracts slightly with decreasing spreading rate which explains the change in the maxima seen in Figure 2. **(b)** Heavy curves represent the maximum in W' as a function of depth for a fixed rate of ridge migration, $U_r = 7$ cm/yr. Light curves are the maxima in W' for $U_r = U_0$.

of depth along the extremal lines. The magnitude of the perturbed upwelling scales with U_r. When $U_r = U_0$, increasing spreading rate is associated with increasing magnitude of W' at all depths (light lines in Figure 4b). The increase in Δd with spreading rate shown in Figure 2 stems from this effect. However, for a fixed U_r, slower spreading results in a larger enhancement of upwelling because slower spreading ridges have a more pronounced thinning of the lithosphere. Finally, the offset at which Δd goes to zero is controlled by the geometry of the base of the lithosphere which limits the width of the region above the solidus. Fast spreading ridges have thinner lids which allow melting due to the perturbed flow to extend further away from the ridge axis.

6. Conclusions

[15] Models described here show that plate-induced mantle dynamics is a plausible explanation for the morphological changes observed along MOR. The perturbation in asthenospheric flow caused by ridge migration generates an asymmetry in melt production rates which, under reasonable assumptions of 3D melt focusing, leads to an asymmetry in predicted axial depth (crustal thickness) across ridge segment boundaries. These results are consistent with models by *Conder et al.* [2002] and *Toomey et al.* [2002] but they do not depend on an inferred large-scale plume-related asthenospheric flow and temperature anomaly. The correspondence between observed and modeled changes in axial depth asymmetry with offset length supports the assumption of plate-driven asthenospheric flow above a high viscosity, zero horizontal velocity mantle. The amplitude of the data can be fit using a conservative estimate of asthenosphere depth and a parametric model of melt focusing. Future models can place better constraints on the scale of melt focusing and upwelling geometry by computing 3D flow and temperature fields.

References

Balay, S., W. D. Gropp, L. C. McInnes, and B. F. Smith (1997), Efficient management of parallelism in object oriented numerical software libraries, in *Modern Software Tools in Scientific Computing*, edited by E. Arge, A. M. Bruaset, and H. P. Langtangen, pp. 163–202, Birkhaüser Boston, Cambridge, Mass.

Balay, S., K. Buschelman, W. D. Gropp et al. (2002), PETSc users manual, *Tech. Rep. ANL-95/11*, rev. 2.1.5, Argonne National Laboratory, Argonne, Ill.

Carbotte, S., C. Small, and K. Donnelly (2004), The influence of ridge migration on the magmatic segmentation of mid-ocean ridges, *Nature*, *429*, 743–746.

Conder, J., D. Forsyth, and E. Parmentier (2002), Asthenospheric flow and asymmetry of the East Pacific Rise, MELT area, *J. Geophys. Res.*, *107*(B12), 2344, doi:10.1029/2001JB000807.

Davis, E., and J. Karsten (1986), On the cause of the asymmetric distribution of seamounts about the Juan de Fuca ridge: Ridge crest migration over a heterogeneous asthenosphere, *Earth Planet. Sci. Lett.*, *79*, 385–396.

DeMets, C., R. Gordon, D. Argus, and S. Stein (1994), Effect of recent revisions to the geomagnetic reversal timescale on estimates of current plate motions, *Geophys. Res. Lett.*, *21*, 2191–2194.

Evans, R., et al. (1999), Asymmetric electrical structure in the mantle beneath the East Pacific Rise at 17 degrees S, *Science*, *286*, 752–756.

Forsyth, D., S. Webb, L. Dorman, and Y. Shen (1998a), Phase velocities of Rayleigh waves in the MELT experiment on the East Pacific Rise, *Science*, *280*, 1235–1238.

Forsyth, D., et al. (1998b), Imaging the deep seismic structure beneath a mid-ocean ridge: The MELT experiment, *Science*, *280*, 1215–1218.

Hirth, G., and D. Kohlstedt (2003), Rheology of the upper mantle and the mantle wedge: A view from the experimentalists, in *Inside the Subduction Factory*, *Geophys. Monogr. Ser.*, vol. 138, edited by J. Eiler, pp. 83–106, AGU, Washington, D. C.

Karato, S., and P. Wu (1993), Rheology of the upper mantle: A synthesis, *Science*, *260*, 771–778.

Katz, R., M. Spiegelman, and C. Langmuir (2003), A new parameterization of hydrous mantle melting, *Geochem. Geophys. Geosyst.*, *4*(9), 1073, doi:10.1029/2002GC000433.

Lin, J., and J. Phipps-Morgan (1992), The spreading rate dependence of three-dimensional mid-ocean ridge gravity structure, *Geophys. Res. Lett.*, *19*, 13–16.

Macdonald, K., P. Fox, L. Perram et al. (1988), A new view of the mid-ocean ridge from the behavior of ridge-axis discontinuities, *Nature*, *335*, 217–225.

Magde, L., and D. Sparks (1997), Three-dimensional mantle upwelling, melt generation, and melt migration beneath segment slow spreading ridges, *J. Geophys. Res.*, *102*, 20,571–20,583.

Richards, M., S. Morris, F. Busse, and A. Lenardic (2003), Towards a physical understanding of the effects of depth-dependent rheology on mantle convection, *EOS Trans. AGU*, *84*(46), Fall Meet. Suppl., Abstract S11G-06.

Schouten, H., H. Dick, and K. Klitgord (1987), Migration of mid-ocean ridge volcanic segments, *Nature*, *326*, 835–839.

Small, C., and L. Danyushevsky (2003), Plate-kinematic explanation for mid-ocean ridge depth discontinuities, *Geology*, *31*(5), 399–402.

Toomey, D., S. Wilcock, S. Solomon et al. (1998), Mantle seismic structure beneath the MELT region of the East Pacific Rise from P and S wave tomography, *Science*, *280*, 1224–1227.

Toomey, D., W. Wilcock, J. Conder et al. (2002), Asymmetric mantle dynamics in the MELT region of the East Pacific Rise, *Earth Planet. Sci. Lett.*, *200*, 287–295.

Turcotte, D., and J. Schubert (2002), *Geodynamics*, 2nd ed., Cambridge Univ. Press, New York.

————————————
S. M. Carbotte, R. F. Katz, and M. Spiegelman, Lamont-Doherty Earth Observatory, Columbia University, 61 Route 9W, Palisades, NY 10964, USA. (katz@ldeo.columbia.edu)